Homodyne Detection of Free Carrier Induced Electro-Optic Modulation in Strained Silicon Resonators

Massimo Borghi, Mattia Mancinelli, Martino Bernard, Mher Ghulinyan, *Member, IEEE, Member, OSA*, Georg Pucker, and Lorenzo Pavesi, *Senior Member, IEEE*

***Abstract*—In the last few years, strained silicon has been proposed as a potential electro-optic material, paving the way to the realization of ultrafast modulators which are compatible with the CMOS fabrication technology. The linear Pockels effect has been used for measuring the magnitude of the induced $\chi^{(2)}$ components, with values reaching hundreds of pm/V. Recently, it has been shown that these values could have been overestimated due to the contribution of free carriers to the electro-optic modulation. In this work, this hypothesis is validated by a series of experimental observations, which are performed on strained silicon racetrack resonators. These are fabricated with different waveguide widths and orientations. We use a low frequency (KHz) homodyne detection technique to monitor the electro-optic response of the devices. The results indicate that the modulation strength is not dependent on the waveguide geometry or direction. A lot of anomalies are encountered in the device response, which are not compatible with a modulation mechanism of $\chi^{(2)}$ origin. To this purpose, a theory based on the nonlinear injection of free carriers inside the waveguide is presented. This is able to account for all the observed anomalies.**

***Index Terms*—Electro-optic effect, homo-dyne detection, racetrack resonator, strained silicon.**

I. Introduction

SILICON has a centrosymmetric crystalline structure, which causes the second order susceptibility to vanish [1]–[3]. The lack of $\chi^{(2)}$-nonlinearities prevented silicon to be promoted as a platform for the realization of ultra-fast electro- optic modulators based on the Pockels effect [4]. More generally, the enabling of a $\chi^{(2)}$ in silicon would benefit from the exploitation of the whole class of second order effects, like Second Harmonic Generation (SHG), Sum Frequency Generation (SFG) and Optical Rectification [5], [6]. These would boost the applications and the engineering possibilities of Silicon Photonics, by constituting a crucial step toward standardization, in which only one material (silicon) and only one fabrication process (CMOS) are used to accomplish an increasingly number of functionalities within the same integrated chip [7], [8]. In the last few years, strained silicon emerged as the most promising solution for the accomplishment this task. Typically, the deposition of a stressing layer of silicon nitride (Si_{3N4}) on the top of the waveguides is used to inhomogeneously deform the lattice structure, thus breaking the inversion symmetry of the material [9]–[14]. The observation of the linear electro-optic effect, i.e., the linear change of the effective index in response to an applied electric field, has been considered so far as the proof of the presence of a strain-induced $\chi^{(2)}$. By using Mach-Zehnder interferometers, in which one of the arms is driven by a static or low frequency (KHz) voltage, the magnitude of some of the $\chi^{(2)}$ tensor components have been extracted, with values ranging from 15 pm/V [9] up to 336 pm/V [13]. However, recent works suggested that there could be a strong contribution of plasma carrier dispersion to the electro-optic modulation, with the consequence that those values could have been overestimated [15]–[17]. In fact, a linear effective index variation of the optical mode of a waveguide can also be induced by free carriers or by trap states and localized charges at the $Si_{3N4} - Si$ interface [15]. In particular, the presence of absorption at high voltages (>100 V), or the observation of an hysteretic behaviour after soaking the material for several minutes at high fields, are strongly indicators of the presence of free carriers accumulated and released from the interfaces [15]. Furthermore, high frequency measurements of the electro-optic effect, performed on strained racetrack resonators, evidenced that the electro-optic modulation monotonically decreases by more than an order of magnitude with respect to the static value, as the time variations of the voltage exceed the free carrier effective lifetime [17].

In this work, we report on a series of experiments on strained silicon racetrack resonators which can be interpreted only if free carriers are assumed to be at the origin of the electro-optic modulation. By exploting the high quality factor of the resonator, in combination with a homo-dyne technique for the detection of the modulation, values of $\chi^{(2)}$ as low as 0.1 pm/V can be revealed. Resonators of different waveguide width and orientations have been fabricated and tested. The experimental results have been classified in two categories. The first includes the devices which have a *normal behaviour*, i.e., with an electro-optic response which has all the features of being induced by a $\chi^{(2)}$. The second includes the ones with an *anomalous* behaviour, which can not be interpreted in terms of $\chi^{(2)}$. We will demonstrate that both normal and anomalous behaviours can be accounted by a

Manuscript received June 21, 2016; revised September 5, 2016 and October 8, 2016; accepted November 9, 2016. Date of publication November 10, 2016; date of current version December 5, 2016. This work was supported by the SIQURO project financed by the Autonomous Provincia of Trento.

M. Borghi, M. Mancinelli, and L. Pavesi are with the Department of Physics, Nanoscience Laboratory, University of Trento, Povo I-38123, Italy (e-mail: massimo.borghi@unitn.it; mattia.mancinelli@unitn.it; lorenzo.pavesi@unitn.it).

M. Bernard, M. Ghulinyan, and G. Pucker are with the Centre for Materials and Microsystems, Fondazione Bruno Kessler, Povo I-38123, Italy (e-mail: bernard@fbk.eu; ghulinyan@fbk.eu; pucker@fbk.eu).

Color versions of one or more of the figures in this paper are available online at http://ieeexplore.ieee.org.

Digital Object Identifier 10.1109/JLT.2016.2628183

theory which relies on the nonlinear injection of free carriers in the waveguide as a consequence of an applied voltage. The paper is organized as follows: in section II, a general theory of the electro-optic response of an Add-Drop resonator subjected to an harmonic voltage is presented. By specializing the theory to $\chi^{(2)}$ nonlinearites, the features of the normal behaviour are derived. Section III presents the fabricated devices and the experimental setup. Sections IV and V detail respectively the experimental evidences of the normal and of the anomalous behaviour. In Sections VI-A and VI-B, the anomalous behaviour is discussed. A unifying theory, which is based on the nonlinear injection of free carriers, and which is capable to interpret both the normal and the anomalous behaviour, is presented in Section VII. A phenomenological interpretation in terms of Surface Transfer Doping (STD) [18]–[20] of carriers at the interface between silicon and Si_{3N4} is introduced at the end of the section.

II. Electro-Optic Response of a Resonator Under an Harmonic Voltage: Theory

Without losing in generality, we will assume a resonator in the Add-Drop filter configuration [21], i.e., a closed loop waveguide which is side coupled to two bus waveguides. A section of the resonator perimeter is subjected to an electric field $\mathbf{E}(t)$, which is induced by a voltage $V(t)$. In the neighbouring of the m^{th} resonance order, the instantaneous Drop intensity $I_D(t)$ is well approximated by the Lorentzian function:

$$I_D(t) = \frac{A\gamma^2}{\gamma^2 + (\lambda - \lambda_m)^2} \tag{1}$$

in which A is the amplitude, 2γ the Full Width at Half Maximum (FWHM), λ the input laser wavelength and λ_m the resonance wavelength. Due to the electro-optic response of the material, the complex effective index becomes dependent on $\mathbf{E}$. In this sense, A, λ_m and γ must be considered functions of V, i.e., $A \rightarrow A(V(t))$, $\lambda_m \rightarrow \lambda_m(V(t))$ and $\gamma \rightarrow \gamma(V(t))$. The dynamics of $I_D(t)$ follows the differential equation:

$$\frac{dI_D}{dt} = \left(\frac{\partial I_D}{\partial \lambda_m}\frac{\partial \lambda_m}{\partial V} + \frac{\partial I}{\partial A}\frac{\partial A}{\partial V} + \frac{\partial I}{\partial \gamma}\frac{\partial \gamma}{\partial V} \right)\frac{dV}{dt} \tag{2}$$

In what follows, the change of the FWHM will be considered a negligible effect compared to the variations of A and λ_m, so it will be neglected. By performing a Taylor expansion of A and λ_m around the reference point $V = 0$, and by considering an harmonic time variation of the voltage $V(t) = V_0 \cos(\omega t)$, one finds:

$$\frac{dI_D}{dt} = -V_0 \omega \sin(\omega t) \sum_q \frac{V^{q-1}}{(q-1)!} \left[\frac{\partial I_D}{\partial \lambda_m}\frac{\partial^q \lambda_m}{\partial^q V}\bigg|_{V=0} + \frac{\partial I_D}{\partial A}\frac{\partial^q A}{\partial^q V}\bigg|_{V=0} \right] \tag{3}$$

For what follows, it is sufficient to keep the terms up to the fourth order in V_0. The result is that, in general, I_D has many harmonic components, each one oscillating at a multiple of the fundamental frequency ω and having an amplitude $I_D(q\omega)$. The two lowest order harmonics $I_D(\omega)$ and $I_D(2\omega)$ are:

$$I_D(\omega) = \frac{\partial I_D}{\partial \lambda_m}\left(\frac{\partial \lambda_m}{\partial V}\bigg|_{V=0} V_0 + \frac{1}{4}\frac{\partial^3 \lambda_m}{\partial^3 V}\bigg|_{V=0} V_0^3 \right) + \frac{\partial I_D}{\partial A}\left(\frac{\partial A}{\partial V}\bigg|_{V=0} V_0 + \frac{1}{4}\frac{\partial^3 A}{\partial^3 V}\bigg|_{V=0} V_0^3 \right) \tag{4}$$

$$I_D(2\omega) = \frac{\partial I_D}{\partial \lambda_m}\left(\frac{1}{2}\frac{\partial^2 \lambda_m}{\partial^2 V}\bigg|_{V=0} V_0^2 + \frac{1}{24}\frac{\partial^4 \lambda_m}{\partial^4 V}\bigg|_{V=0} V_0^4 \right) + \frac{\partial I_D}{\partial A}\left(\frac{\partial^2 A}{\partial^2 V}\bigg|_{V=0} V_0^2 + \frac{1}{24}\frac{\partial^4 A}{\partial^4 V}\bigg|_{V=0} V_0^4 \right) \tag{5}$$

The dependence of $I_D(\omega)$ and $I_D(2\omega)$ on the input laser wavelength λ is described by the functions $\frac{\partial I_D}{\partial \lambda_m}$ and $\frac{\partial I_D}{\partial A}$. These have opposite symmetry with respect to λ_m, in particular $\frac{\partial I_D}{\partial \lambda_m}$ has an odd symmetry while $\frac{\partial I_D}{\partial A}$ has an even symmetry. These considerations will be crucial for understanding the anomalous device response described in section VI-A. The Pockels effect does not introduce changes in the material absorption (apart from the Franz-Keldysh effect [23], which at the wavelength of 1.55 μm, at which the device is considered to operate, can be neglected), so $\frac{\partial^q A}{\partial^q V} = 0$ for all q. We can now apply the general expressions of (4), (5) to the case of the $\chi^{(2)}$ electro-optic modulation, i.e., the linear Pockels effect. In this case, the change of the effective index Δn_{eff} induced by the applied electric field $\mathbf{E} = E\hat{j}$ ($\hat{j}$ could represent any of the (x, y, z) directions of space) is given by [22]:

$$\Delta n_{\text{eff}} = \frac{\chi^{(2)}_{\text{eff,jjj}} E n_g}{2n_0^2} \tag{6}$$

in which n_g is the modal group index, n_0 is the material refractive index and $\chi^{(2)}_{\text{eff,jjj}}$ is the modal averaged effective $\chi^{(2)}$, defined as:

$$\chi^{(2)}_{\text{eff,jjj}} = \frac{\int_{wg} \chi^{(2)}_{\text{mat,jjj}}(\mathbf{x}_t) n^2(\mathbf{x}_t) |e_j(\mathbf{x}_t)|^2 d\mathbf{x}_t}{\int n^2(\mathbf{x}_t) |\mathbf{e}(\mathbf{x}_t)|^2 d\mathbf{x}_t} \tag{7}$$

in which $\chi^{(2)}_{\text{mat,jjj}}$ is the strain induced $\chi^{(2)}_{\text{jjj}}$ component inside the material, n is the refractive index distribution , $\mathbf{e}(\mathbf{x}_t)$ is the modal electric field profile and $\mathbf{x}_t$ denotes the transverse coordinates with respect to the light propagation direction. In deriving (6), (7), the optical and the applied electric fields have been assumed completely co-polarized along the $\hat{j}$ direction, so as off-diagonal tensor terms do not contribute to the effective $\chi^{(2)}$. It is worth to note that the whole theory holds even if the optical and the applied electric fields are cross-polarized. In this case, it is sufficient to replace the diagonal element $\chi^{(2)}_{\text{jjj}}$ of the $\chi^{(2)}$ tensor with the off-diagonal one $\chi^{(2)}_{\text{ijj}}$, with $i \neq j$. The

change in the effective index Δn_{eff} induces a resonance shift:

$$\Delta\lambda_m = \lambda_m \frac{\Delta n_{\text{eff}} \eta}{n_g} \tag{8}$$

in which η is the fraction of the resonator perimeter in which the change in effective index occurs. By combining together (6)–(8) into (4), (5) one obtains:

$$I_D(\omega) = \frac{\partial I_D}{\partial \lambda_m} \frac{\lambda_m \eta \chi^{(2)}_{\text{eff,jjj}}}{2n_0^2} \frac{dE}{dV}\bigg|_{V=0} V_0$$

$$I_D(2\omega) = 0 \tag{9}$$

In (9), the electric field has been assumed to depend linearly with the applied voltage, as $E = (\frac{dE}{dV})V$. This holds if the material is considered as a perfect insulator, in which the field is not screened by free charges. The fact that $I_D(2\omega)$ is equal to zero is a consequence of the linearity of the $\chi^{(2)}$-Pockels effect. Eq. (9) can be considered as the basic equation for defying the *normal* behaviour of a device. In case that the electro-optic modulation is due to $\chi^{(2)}$ effects, $I_D(\omega)$ must vary linearly with the amplitude of the applied sinusoidal voltage. No higher order harmonics should be observed. Moreover, $I_D(\omega)$ must be an odd function of the input laser wavelength. The devices with an electro-optic response which deviates from the predictions of (9) are considered to have an *anomalous* behaviour. The amplitude of the different harmonics in the dropped intensity can be extracted by using an homo-dyne detection technique, as described in section III.

III. Devices and Experimental Setup

We fabricated the Add-Drop resonators on a 6″ Silicon On Insulator (SOI) wafer using 365 nm UV lithography. An optical microscope image is shown in Fig. 1(a).

A silicon nitride (Si_{3N4}) layer of thickness 140 nm is conformally deposited on the silicon waveguides by Low Pressure Chemical Vapour Deposition. A 3 μm buried oxide layer and a 900 nm thick Plasma Enhanced Chemical Vapour Deposition silica layer serve as lower and upper cladding materials, respectively. Wafer bow measurements evidenced a compressive stress of -190 MPa on the silica layer. Since this value is low compared to the ones reported in literature for similar works (see, e.g., Refs. [10], [11], [13]), some of the samples have been fabricated without the silica top cladding, which partially absorbs the stress induced by the Si_{3N4}. In this case, the bow measurement revealed a compressive stress of -1.4 GPa. The waveguides have a cross section of (width $\times$ height) 400 nm $\times$ 250 nm. In the region where the electric field is applied, the width of the waveguides is increased using adiabatic tapers, which preserve the single mode operation. The final waveguide width w ranges from 400 nm to 4 μm, and is increased using steps of 400 nm. The perimeter of the resonator is 415 μm. The coupling coefficient with the two bus waveguides ranged from $\kappa^2 = 0.07$ to $\kappa^2 = 0.025$. Two sets of Aluminium electrodes, of length 50 μm, are deposited on the top of the large waveguide sections to apply the electric field. One set (indicated as Electrodes Z-Field in Fig. 1(a)) is used to apply an electric field oriented in the $\hat{z}$ direction. This is achieved by grounding the two external

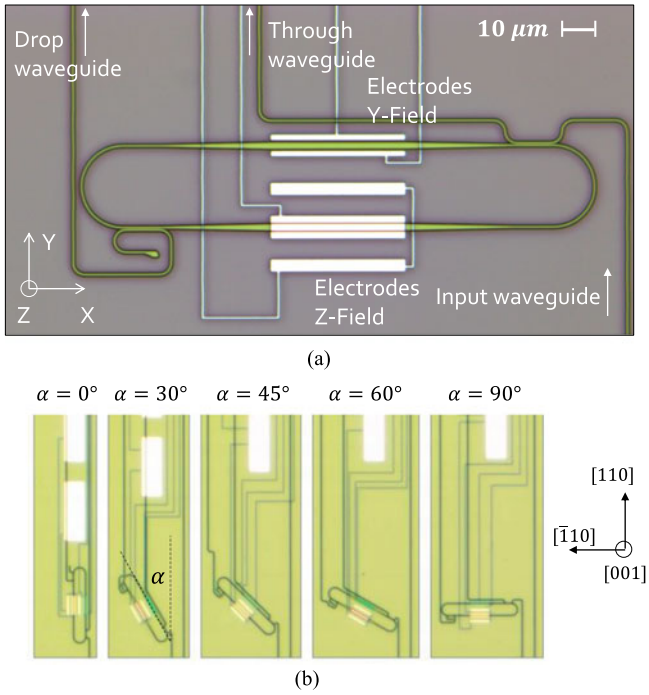

Fig. 1. (a) Optical microscope image of a fabricated racetrack device. Indicated are the Input port, where light is injected from the outside, and the Drop and the Through waveguides, where light is collected. Electrodes appear in white. The Tungsten tips are applied to metallic pads which lie outside the figure. (b) Optical microscope image of the racetrack in different orientations.

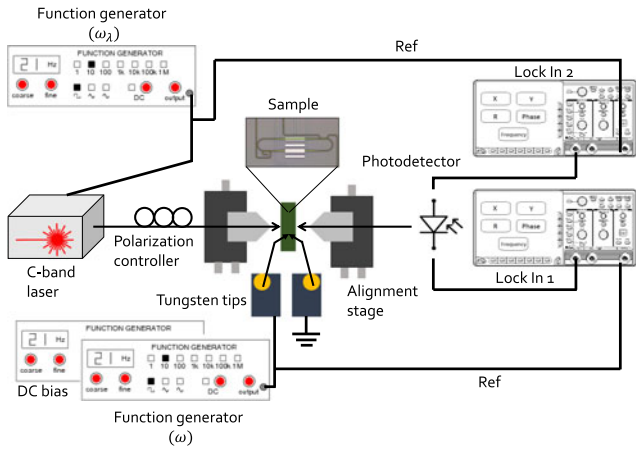

Fig. 2. Sketch of the experimental setup used for probing the electro-optic response of the resonators.

electrodes and by applying a voltage to the central one. This configuration is used for the devices with a silica top cladding. The other set (indicated as Electrodes Y-Field in Fig. 1(a)) applies the field in the $\hat{y}$ direction. This configuration is used with the devices without the silica top cladding. The resonators have been fabricated with different orientations, corresponding to five different tilting angles α, which are $\alpha = (0°, 30°, 45°, 60°, 90°)$. As shown in Fig. 1(b), this angle is referred between the [110] crystallographic direction and the light propagation direction in the straight sections. In the case $\alpha = 0$, the two directions coincide. To probe the device electro-optic response, the experimental setup shown in Fig. 2 has been used.

Light from a tunable C-band laser is edge coupled to the input waveguide using tapered lensed fibers and a XYZ micrometric and nanometric positioning stage. A polarization controller is used to set the light polarization to Transverse Magnetic (TM), which in Fig. 1(a) correspond to an optical field mainly polarized in the $\hat{z}$ direction. The output light from the Drop (Through) waveguide is edge coupled to another lensed fiber and sent to an Infra-Red detector. To provide the electric field across the metallic electrodes of the devices, two Tungsten tips connected to a function generator have been u sed. This generates the sinusoidal voltage at frequency $\nu = \frac{\omega}{2\pi} = 1.6$ KHz. A static bias can be added to the harmonic modulation using an auxiliary voltage source. The electronic signal which exits from the photodetector is sent to a digital Lock In amplifier to detect the amplitude of the first and of the second harmonic components $I_D(\omega)$ and $I_D(2\omega)$. A second Lock In is used to detect the local spectral slope $\frac{\partial I_D}{\partial \lambda_m}$, which is essential for extracting the value of the $\chi^{(2)}$ using (9). To this purpose, the laser wavelength is periodically modulated at a frequency $\nu_\lambda = \frac{\omega_\lambda}{2\pi} = 1.2$ KHz using an external trigger which drives the C-band laser. The whole setup is automated by a computer routine which, in order:

1) Performs a coarse spectrum (0.1 nm resolution) in a wavelength interval which covers approximately one free spectral range.
2) Finds the resonance peak in the interval, performs a fine spectra (5 pm resolution) around the maximum value and sets the laser wavelength at the point where the slope of the spectrum is maximum. This is where the resonator has the highest sensitivity to effective index variations.
3) Applies a modulated voltage across the pads, starting from an amplitude of $V_0 = 0.35$ V to $V_0 = 7$ V, with 0.35 V increments, and simultaneously detects the amplitude of $I_D(\omega)$ and $I_D(2\omega)$.
4) Extracts the value of $\chi^{(2)}_{\text{eff},zzz}$ using (9). The parameters η, n_0 and $\frac{dE}{dV}$ are respectively taken from the geometric design, from [24] and from Finite Element Method simulations.
5) Shifts to the next resonance order and repeats the points 3 and 4. This is repeated for 3 consecutive resonance orders for each device.

The minimum detectable signal of our measuring apparatus corresponds to a value of $\chi^{(2)}_{\text{eff},zzz}$ of 0.1 pm/V.

IV. Normal Behaviour

The amplitudes $I_D(\omega)$ and $I_D(2\omega)$ for a device showing a normal behaviour are reported in Fig. 3(a). As predicted from (9), an electro-optic modulation which is induced by a $\chi^{(2)}$ nonlinearity must have a first harmonic amplitude which is linear in V_0, and vanishing higher order harmonics. This is actually what emerges from Fig. 3(a). When $I_D(\omega)$ is monitored as a function of the wavelength, keeping the amplitude of the modulation voltage fixed to $V_0 = 5$ V, the response shown in Fig. 3(b) (which is relative to the sample with $w = 0.8$ μm, $\alpha = 30^\circ$) is observed. This electro-optic response has almost an odd symmetry with respect to the resonance wavelength $\lambda_m = (1510.50 \pm 0.02)$ nm, which is expected because $I_D(\omega)$ is proportional to the local

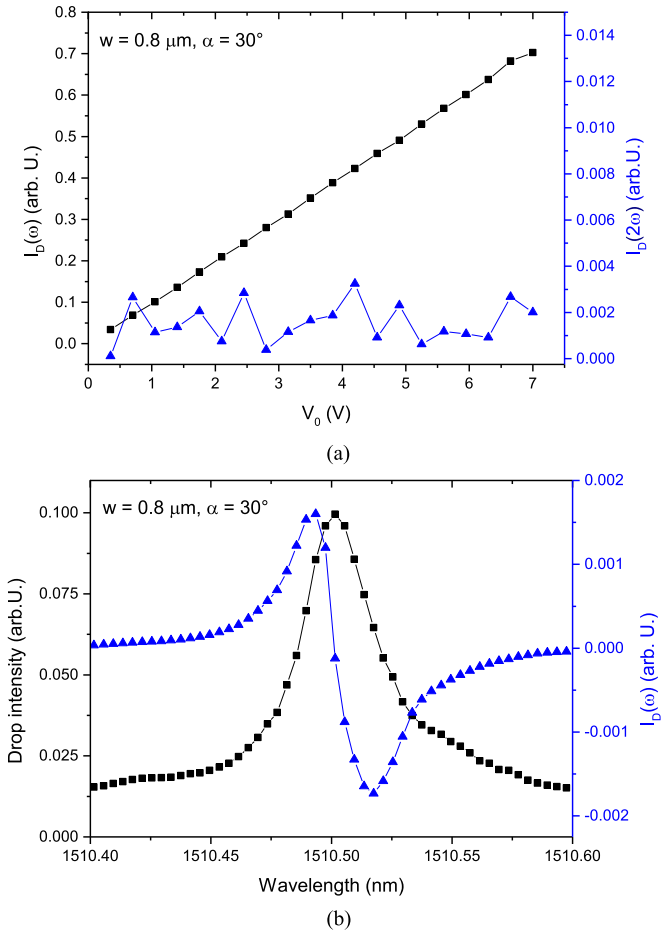

Fig. 3. (a) First and second harmonic amplitudes as a function of V_0. (b) Spectrum and first harmonic amplitude as a function of the wavelength, with $V_0 = 5$ V.

slope of the spectrum $\frac{\partial I_D}{\partial \lambda_m}$. We point out that small deviations from a perfect odd symmetry can be attributed to the reflections at the input/output facet of the sample, which alter the local slope $\frac{\partial I_D}{\partial \lambda_m}$ of the resonator spectral response [25]. This effect is visible in Fig. 3(b), where the resonance lineshape appears slightly distorted, and thus departs from a perfectly symmetric Lorentzian lineshape. Starting from curves similar to the ones shown in Fig. 3(a), we extracted the values of $\chi^{(2)}_{\text{eff},zzz}$ for resonators having different waveguide widths w and tilting angles α. These are reported in Fig. 4. The values of the extracted $\chi^{(2)}_{\text{eff},zzz}$ range from a minimum of few pm/V up to 600 pm/V. Each point in Fig. 4 is the result of an average of the $\chi^{(2)}_{\text{eff},zzz}$ values obtained for three consecutive resonance orders. Error bars are mainly associated to the reflections at the input/output facet of the sample, which alter the local slope $\frac{\partial I_D}{\partial \lambda_m}$ of the resonator spectral response. The averaging over multiple resonance orders helps to reduce this source of uncertainly. By inserting the values of the $\chi^{(2)}_{\text{eff},zzz}$ shown in Fig. 4 into (6)–(8), it is possible to estimate that the modulation amplitude of the resonance wavelength, induced by the sinusoidal voltage, lies between 0.1 pm and 0.5 pm. By looking at Fig. 4, we can recognize several anomalies in the extracted values of the $\chi^{(2)}_{\text{eff},zzz}$. Firstly, there is not a precise trend with

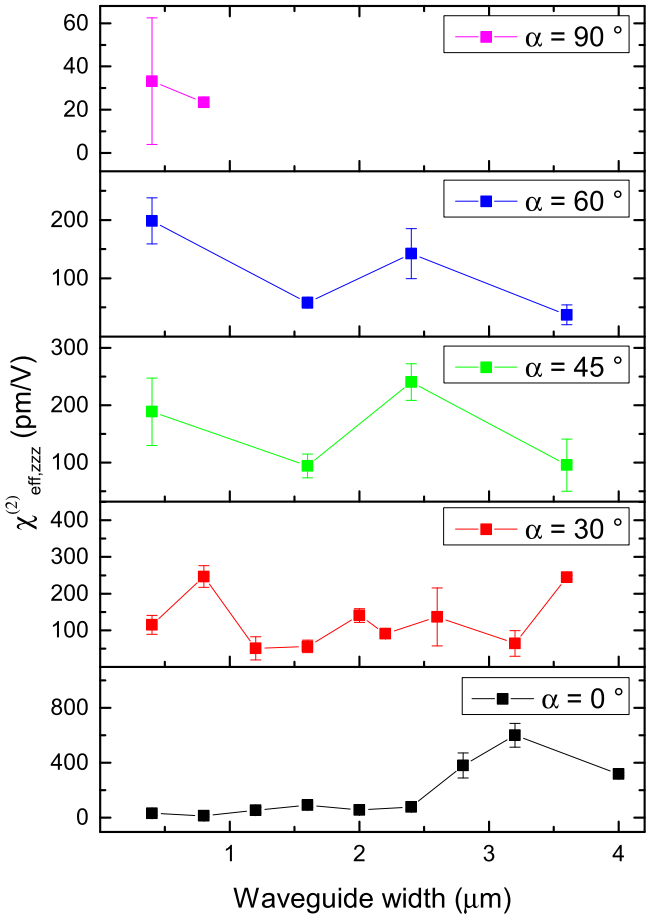

Fig. 4. Values of $\chi^{(2)}_{\mathrm{eff},zzz}$ for resonators having different waveguide widths and different tilting angles α. The values of $\chi^{(2)}_{\mathrm{eff},zzz}$ are extracted as detailed in section III.

the waveguide width, or with the waveguide tilting angle. FEM simulations show that the magnitude of the stress (hence strain) distribution in the core region depends on the waveguide width. In particular, the average strain gradient is expected to decrease as the waveguide width increases, and consequently, also the $\chi^{(2)}_{\mathrm{eff},zzz}$ should decrease [1]. Secondly, there is no clear dependence with the device orientation. This is in contrast with the fact that the stress distribution is strongly anisotropic (see e.g., [10], [14]), which should be reproduced in the tensor properties of the induced $\chi^{(2)}_{\mathrm{eff},zzz}$. Furthermore, the value of the nonlinearity can be as high as 600 pm/V, which is much greater than the ones reported in literature for similar geometries [10]–[13]. Surprisingly, this high value has been found with a stress level of -190 MPa, which is one order of magnitude lower than the one in the above cited works. Similar trends, with comparable $\chi^{(2)}_{\mathrm{eff},zzz}$ values, have been found in samples without the silica top cladding. In these cases, the stress is -1.4 GPa, and the probed component is the $\chi^{(2)}_{\mathrm{eff},yzz}$ (static field polarized along the $\hat{y}$ direction and optical field set in the fundamental TM mode). The remarkable difference which has been found in samples without the Si_{3N4} cover, is that the strength of the electro-optic modulation was lower by approximately one order of magnitude with respect to the covered samples.

V. Anomalous Behaviour

The strangeness encountered in the trends of Fig. 4 are supported by the observation of anomalous behaviours in some devices. We will start by considering the electro-optic responses which violates the symmetry in wavelength predicted by (9). To this purpose, a static bias V_{DC} is added to the harmonic voltage applied to the electrodes, and $I_D(\omega)$ is monitored at a fixed V_0, while the laser wavelength is swept. An example of anomalous result, relative to a device with $w = 400$ nm and $\alpha = 0$, is shown in Fig. 5(a) and (b). We see that by changing V_{DC}, it is possible to tune the degree of asymmetry Γ of the electro-optic response in wavelength. This quantity is defined as:

$$\Gamma = \int I_D(\omega, \lambda) d\lambda \tag{10}$$

The value of Γ, for different bias voltages, is reported in Fig. 5(c). From (9), one can see that the asymmetry should be always equal to zero, independently on the value of the static bias. It is evident from Fig. 5(a) and (c) that a theory which relies only on $\chi^{(2)}$ nonlinearities is not able to reproduce these electro-optic responses. The value of V_{DC} at which $\Gamma = 0$ is found to be sample dependent. In some cases, this can be as high as $\pm(30 \div 40)$ V. Another anomaly is encountered in the relation between the first or the second harmonic amplitude and V_0. An example, relative to a device with $w = 1.2$ μm and $\alpha = 0°$, is shown in Fig. 6(a). In this case, the linear relation between $I_D(\omega)$ and V_0, predicted by (9), holds only for small voltage amplitudes. When $V_0 > 1$ V, the relation becomes cubic. In parallel, the amplitude of $I_D(2\omega)$ quadratically increases with V_0. This means that the electro-optic effect is no more linear with the applied voltage, since a frequency doubled signal is created in the transmitted output intensity.

All the reported anomalies seem to not have a clear relationship either with the waveguide width, or with the device orientation. It is worth to note that, in some cases, two nominally identical samples have been found to have a normal behaviour and an anomalous behaviour depending on their position on the wafer.

VI. Interpretation of the Anomalous Behaviour

A. Interpretation of the Symmetry in Wavelength

In order to account for the violation of the odd symmetry in wavelength, one has to refer to (4), in which both the resonance wavelength λ_m and the amplitude A are affected by the driving voltage. This implies that losses are introduced as a consequence of the applied voltage. For the following considerations, it is sufficient to keep in consideration only the terms which are linear in V_0, thus obtaining:

$$I_D(\omega) = \left(\frac{\partial I_D}{\partial \lambda_m} \frac{\partial \lambda_m}{\partial V} \bigg|_{V=0} + \frac{\partial I_D}{\partial A} \frac{\partial A}{\partial V} \bigg|_{V=0} \right) V_0 \tag{11}$$

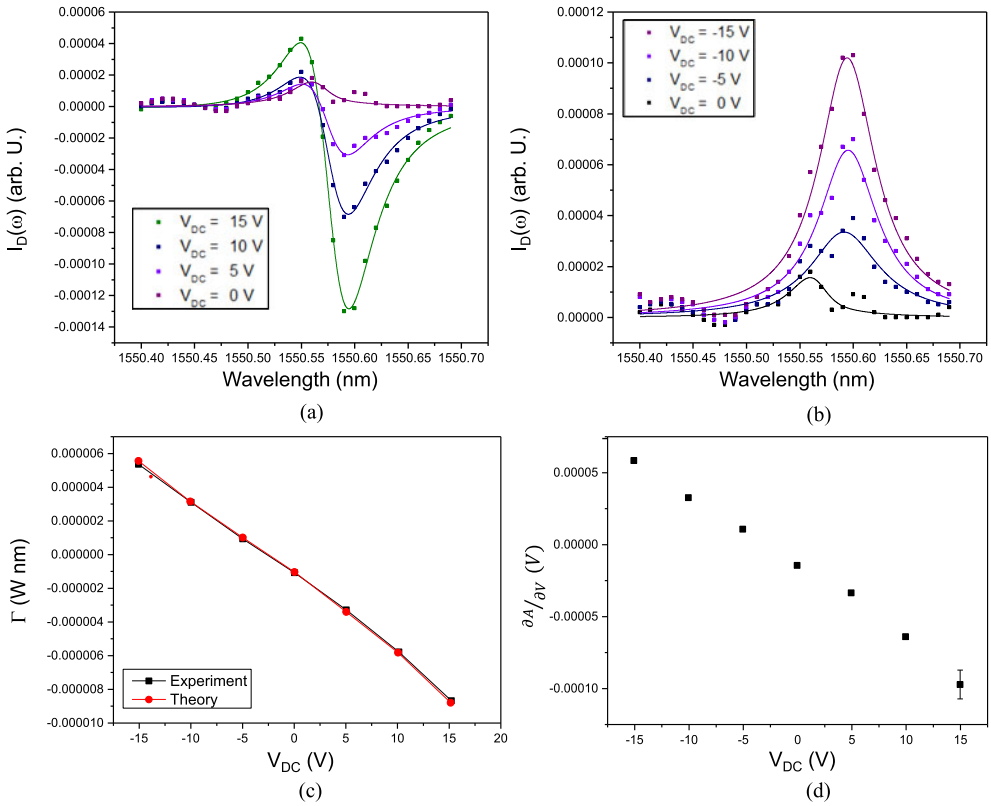

Fig. 5. (a) First harmonic amplitude as a function of wavelength for different values of positive applied voltages. Scatter points represent experimental data, while solid lines are obtained using (11). (b) First harmonic amplitude as a function of wavelength for different values of negative applied voltages. (c) Asymmetry parameter Γ, defined in (10), plotted as a function of the bias voltage V_{DC}. The black line is obtained by directly integrating $I_D(\omega)$ with respect to λ on the experimental data. The red line is obtained by integrating the solid curves in panels (a),(b) with respect to λ. (d) Values of $\frac{\partial A}{\partial V}$ for different bias voltages. For simplicity, in computing the value of $\frac{\partial A}{\partial V}$, the quantity $\frac{\partial I_D}{\partial A}$ has been assumed normalized to one.

The addition of the second term on the right hand side makes (11) a function with undefined symmetry. By integrating (11) with respect to the wavelength, the asymmetry parameter Γ results to be proportional to $\frac{\partial A}{\partial V}$. Since, as can be seen from Fig. 5(c), the value of Γ can be tuned with the bias voltage V_{DC}, we must conclude that the amount of losses which are introduced in response to the applied field are voltage dependent. (11) is used to fit the experimental data of Fig. 5(a) and (b). During this procedure, the quantities $\frac{\partial I_D}{\partial \lambda_m}$ and $\frac{\partial I_D}{\partial A}$ have been assumed normalized to one. In general, there is a very good agreement between theory and experiment. The extracted values from the fit of $\frac{\partial A}{\partial V}$ are reported in Fig. 5(d).

B. Interpretation of the Cubic Response

The cubic relation between $I_D(\omega)$ and V_0 is actually predicted by (4). This requires that $\frac{\partial^3 \lambda_m}{\partial^3 V}$ is not equal to zero, i.e., that electro-optic shift of the resonance wavelength is cubic with the applied voltage. In the same way, the first nonlinear correction to the second harmonic amplitude $I_D(2\omega)$ is quadratic in V_0, which is exactly what emerges from Fig. 6(b). In section II, it has been demonstrated that, in a theory in which the electro-optic modulation is due to a purely $\chi^{(2)}$ effect, and in which the core material is considered as a perfect insulator, the relation between λ_m and V_0 is linear. By breaking these two assumptions, this condition can be relaxed. We will now demonstrate that one has necessarily to include the presence of free carriers in order to explain the behaviour shown in Fig. 6(a) and (b). Indeed, the only plausible origin of a nonlinear electro-optic modulation, which does not rely on free carriers, is the $\chi^{(3)}$-mediated quadratic electro-optic effect [12]. In this case, the effective index shift in (6) gets an additional term [22]:

$$\Delta n_{\text{eff}} = \frac{\chi^{(2)}_{\text{eff,jjj}} n_g E}{2n_0^2} + \frac{9\chi^{(3)}_{\text{eff,jjjj}} n_g E^2}{16 n_0^2} \tag{12}$$

in which the effective $\chi^{(3)}$ is defined as:

$$\chi^{(3)}_{\text{eff,jjjj}} = \frac{\int_{wg} \chi^{(3)}_{\text{mat,jjjj}}(\mathbf{x}_t) n^2(\mathbf{x}_t) |e_j(\mathbf{x}_t)|^2 d\mathbf{x}_t}{\int n^2(\mathbf{x}_t) |\mathbf{e}(\mathbf{x}_t)|^2 d\mathbf{x}_t} \tag{13}$$

and $\chi^{(3)}_{\text{mat,jjjj}}$ denotes the $\chi^{(3)}_{\text{jjjj}}$ component inside the material. It is straightforward to demonstrate that the inclusion of the quadratic Pockels effect in (4), (5) can only justify the quadratic relation between $I_D(2\omega)$ and V_0, but not the cubic one between $I_D(\omega)$ and V_0. Indeed, insertion of (12) into (6)–(8) gives (neglecting the terms in A):

$$I_D(2\omega) = \frac{9\lambda_m \chi^{(3)}_{\text{eff,jjjj}} \eta}{8 n_0^2} \left(\frac{\partial E}{\partial V} \right)^2 V_0^2 \tag{14}$$

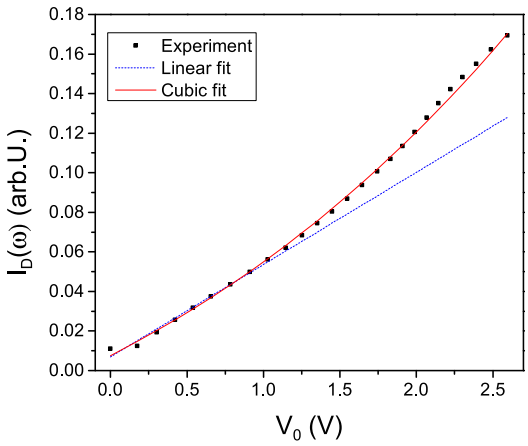

Fig. 6. (a) Anomalous behaviour of the first harmonic $I_D(\omega)$. Black scatters represent the experimental data, the red line is the polynomial $I_D(\omega) = a_0 + a_1 V_0 + a_3 V_0^3$, while the blue line is the polynomial $I_D(\omega) = b_0 + b_1 V_0$. (b) Anomalous behaviour of the second harmonic $I_D(2\omega)$ as a function of the voltage amplitude V_0. Black scatters represent the experimental data, while the solid red line is a quadratic polynomial $I_D(2\omega) = c_0 + c_1 V_0^2$. The values of the coefficients are listed in Table I.

while the expression for $I_D(\omega)$ remains the same of (9). To obtain the cubic relation, one must introduce a nonlinear relationship between the voltage and the field. At lowest order, one can consider the quadratic form $E = E_0 + c_1 V + c_2 V^2$, in which E_0 is a frozen electric field in the material (which can be due to a surface charge layer at the Si_{3N4} interface [26]), while c_1 and c_2 are constants. By inserting this quadratic dependence into (12), we have that (4), (5) become:

$$I_D(\omega) = (K_1 c_1 + 2K_2 c_1 E_0) V_0 + 12 K_2 c_1 c_2 V_0^3 \quad (15)$$

$$I_D(2\omega) = (2K_2 c_1^2 + 2K_2 c_2 + 4K_2 E_0 c_2) V_0^2 \quad (16)$$

in which K_1 and K_2 are defined as:

$$K_1 = \frac{\lambda_m \eta \chi^{(2)}_{\text{eff,jjj}}}{2n_0^2}$$

$$K_2 = \frac{9\lambda_m \eta \chi^{(3)}_{\text{eff,jjjj}}}{16 n_0^2} \quad (17)$$

TABLE I
VALUES OF THE COEFFICIENTS OF THE POLYNOMIALS USED TO FIT THE EXPERIMENTAL DATA SHOWN IN FIG. 6

Coefficient	Value
a_0	(-0.07 ± 0.01) W
a_1	(0.019 ± 0.007) WV^{-1}
a_3	$(7.6 \pm 0.6) \cdot 10^{-4}$ WV^{-3}
b_0	(-0.133 ± 0.007) W
b_1	(0.047 ± 0.002) WV^{-1}
c_0	(0.037 ± 0.003) W
c_2	(0.030 ± 0.008) WV^{-2}

TABLE II
VALUES OF THE PARAMETERS USED TO EVALUATE THE CUBIC CORRECTION OF (15)

Parameter	Value	Reference
V_0	2.5 V	Experiment
$\chi^{(2)}_{\text{eff,jjj}}$	10^2 pm/V	[11]
$\chi^{(3)}_{\text{eff,jjjj}}$	$10^{-18}\ \frac{\text{m}^2}{\text{V}^2}$	[12]
c_2	518 cm^{-1} V^{-1}	FEM simulation

In order to have $c_2 \neq 0$, the core material should not be a perfect insulator. Carriers must be free to be injected and redistributed in response to an applied voltage in order to screen the electric field inside the material. Note that, even if at this stage we are introducing the presence of free carriers, we are still neglecting their contribution in terms of effective index shift in (15), (16). In Appendix A, it is demonstrated that a reasonable value for c_2 is of the order of $\simeq 500$ cm^{-1}V^{-1}. The order of magnitude of the cubic correction in Eq.15 is of the order of $\simeq \frac{V_0^2 K_2 c_2}{K_1}$. By assuming the reasonable set of parameters listed in Table II, which are meaningful for the experimental conditions at which the curves shown in Fig. 6(a) and (b) are obtained, the cubic correction induced by the quadratic Pockels effect is $\sim 10^{-5}$. However, from the parameters shown in Table I, we see that the cubic correction is actually $\frac{(a_3 V_0^2)}{a_1} \sim 10^{-1}$. This means that the presence of $\chi^{(3)}$ nonlinearities alone can not quantitatively account for the anomalous behaviour shown in Fig. 6(a).

VII. THE FREE CARRIER INTERPRETATION

The presence of voltage induced absorption strongly suggests that free carriers are at the origin of the electro-optic modulation. To quantitatively prove this, we applied to the resonators DC voltage, and we monitored at the same time the shift of the resonance wavelength and the change in the quality factor Q. The results, relative to a resonator with $w = 1.2$ μm and $\alpha = 0^\circ$, are shown in Fig. 7(a) and (b).

Two important features emerge from this analysis. The first is that the magnitude of the resonance shift is related to the induced losses. Higher shifts are associated to higher losses. At $V_{DC} =$ 70 V, the decrease of the quality factor is (-0.16 ± 0.05) dB, while the resonance shift is $\Delta\lambda = (-10.10 \pm 0.09)$ pm. The presence of the voltage induced absorption can be appreciated

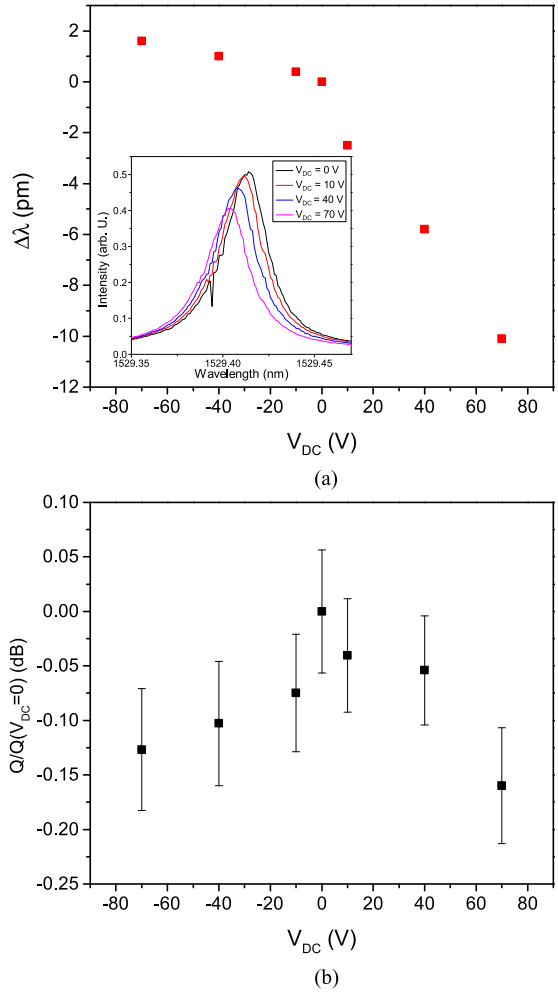

Fig. 7. (a) Shift of the resonance wavelength $\Delta\lambda = \lambda_m(V_{DC}) - \lambda_m(V_{DC} = 0)$ as a function of the static voltage V_{DC}. The inset show the Drop spectral response at the different values of positive V_{DC}. (b) Quality factor of the resonance as a function of the static voltage. The Q-factor is normalized with respect to the value at $V_{DC} = 0$

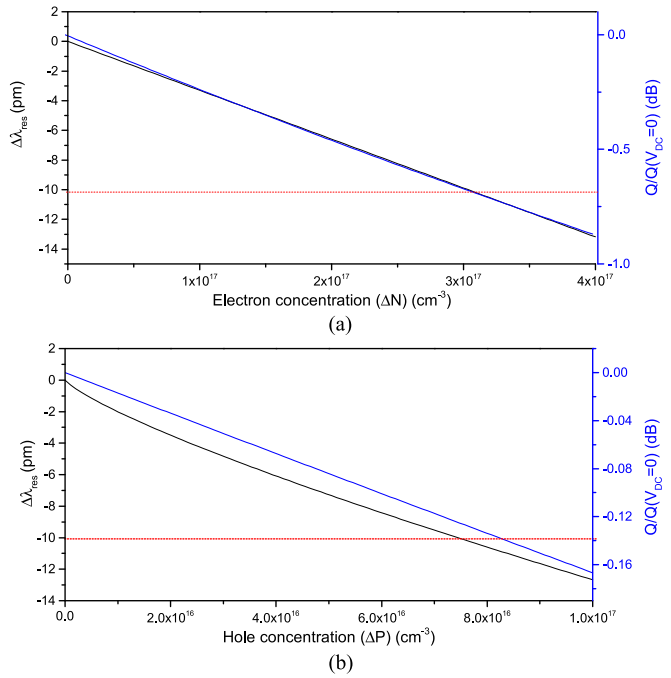

Fig. 8. (a) Shift of the resonance wavelength $\Delta\lambda = \lambda_m(V_{DC}) - \lambda_m(V_{DC} = 0)$ (black line) and normalized quality factor decrease (blue line) as a function of the injected electron concentration. (b) Shift of the resonance wavelength (black line) and normalized quality factor decrease (blue line) as a function of the injected hole concentration. In both panels, the red dashed line represents the experimental value of $\Delta\lambda$ when $V_{DC} = 70$ V.

also in the inset of Fig. 7(a), in which it is shown that the maximum intensity of the transmitted optical signal decreases as the applied voltage increases. The second is that the resonance shift is asymmetric with respect to the sign of the applied voltage ($|\Delta\lambda| < 2$ pm at $V_{DC} = -70$ V, while $|\Delta\lambda| > 10$ pm at $V_{DC} = 70$ V). Since the change in the effective index and in the absorption coefficient induced by free carriers are quantitatively related by the Soref's equations [27], one should expect a similar relation between the resonance shift and the induced losses in the measured electro-optic response. To prove this, we simulated the resonance shift and the decrease of the quality factor as a function of the free carrier concentration injected into the waveguide (details are given in Appendix B). The results of the simulation are shown in Fig. 8(a) and (b). Theory and experiment agrees if the injected carriers are holes. Indeed, a concentration of $(7.67 \pm 0.01) \cdot 10^{16}$ cm^{-3} produces a resonance shift of (-10.10 ± 0.01) pm and a quality factor decrease of (-0.12 ± 0.01) dB with respect to the zero bias condition, which are both compatible with the values found in the experiment.

A. Interpretation of the Normal Behaviour in Terms of Free Carriers

In Sections VI-A and VI-B, we demonstrated that the anomalous behaviour can not be interpreted in terms of $\chi^{(2)}$ nonlinearities, and that one has necessarily to introduce free carriers to justify the experimental observations. The question which now arises is what is happening in the devices which show a normal behaviour. Indeed, their electro-optic response (see, e.g., Fig. 3(a) and (b)), is both compatible with the Pockels effect and with free carrier dispersion. One way to tell the origin of the modulation could be to apply a static voltage bias to the electrodes, as it was done in Fig. 5, and see if the electro-optic response can turn from normal to anomalous. Unfortunately, we found out that this approach was not helpful, since in many devices we were not able to induce any appreciable asymmetry by changing the bias condition. Hence, for some devices, it has been impossible to determine the origin of the modulation from their AC electro-optic response. Nevertheless, by monitoring the amplitude and the quality factor of the resonance as a function of the bias voltage, (see, e.g., Fig. 7), we observed a change in the absorption coefficient for all the measured devices. This made us to conclude that both the normal and the anomalous electro-optic response must have a common origin, which is the free carrier dispersion. The reason why it is possible to tune the asymmetry in only some devices relies on the type of carriers which are responsible for the electro-optic modulation. To clarify this concept, we used (11) to simulate the first harmonic amplitude as a function of the wavelength and of the DC

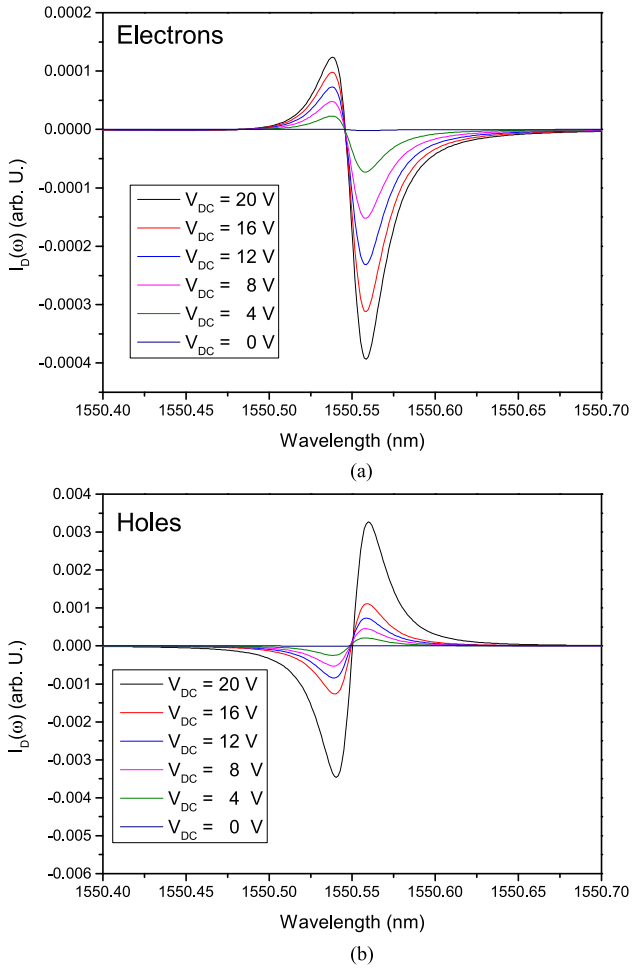

Fig. 9. Simulation of the first harmonic amplitude $I_D(\omega)$ as a function of wavelength for different bias voltages V_{DC}. In panel (a), the injected carriers are electrons, while in panel (b) the injected carriers are holes.

bias, in order to reproduce the trends observed in Fig. 5. In our simulations, we assumed that free carriers are injected into the waveguide as a consequence of the applied voltage (details are given in Appendix B). In Fig. 9(a), it is shown the electro-optic response in case of electrons, while in Fig. 9(b) the injected carriers are holes. In these simulations, the injection is assumed to be unipolar, so only holes (Fig. 9(b)) or electrons (Fig. 9(a)) are separately injected. At this stage, we do not care about how these carriers are injected with the applied voltage. It is evident that a strong tunable asymmetry exists only for electrons. This difference is explained from the fact that, if the same carrier concentration is injected into the waveguide, the ratio between the change in the absorption coefficient and the variation in the refractive index is approximately four times higher for electrons with respect to holes. This makes the second term on the right hand side of (11) to be of the same order of magnitude of the first term, thus strongly contributing to the asymmetry of $I_D(\omega)$. This effect is approximately four times weaker for holes, which makes the asymmetry of the first harmonic amplitude to be very small and almost insensitive to the DC bias. The tunability of the asymmetry of $I_D(\omega)$ can then be used as a tool for distinguishing the type of carriers which are injected into the waveguide. We point out that this result is not in contradiction with the ones of Fig. 8, in which it is blamed that only the injection of holes can justify the experimental observations. This is because the two results refer to different samples, and accordingly to what it will be stated in Section VII-B, the type of injected carrier can vary from sample to sample depending on the nature of the carried trap states located at the interface between Si and Si_{3N4}.

B. Injection Mechanism Inside the Waveguide

Up to now, it has not been discussed how carriers are injected into the waveguide. This is surrounded by silica, which is an electrical insulator, so carriers can not be injected from the outside. The oxide thickness on the top of the waveguide is 900 nm, which precludes tunneling of carriers through this layer. One can then infer that the change in the absorption and in the refractive index comes from a redistribution of the carriers inside the waveguide core as a consequence of the applied electric field. This phenomenon has been investigated through FEM simulations. We simulated the carrier distribution at equilibrium when a voltage is applied through the electrodes, and from this we computed the change in the effective index Δn_{eff} for the fundamental TM mode. Depending on the waveguide width, the variation ranged from 10^{-7} to 10^{-6} when ± 70 V are applied. By plugging this effective index variation into 8, the predicted resonance shift induced by carrier redistribution is about $10^{-3} \div 10^{-2}$ pm. This value is two orders of magnitude lower than the minimum resonance shift observed for any device when ± 70 V are applied, which means that the impact of carrier redistribution in the total effective index change is negligible. By virtue of this fact, the most plausible explanation of the origin of the carrier injection relies on Surface Transfer Doping (STD) between silicon and the Si_{3N4} interface [20]. STD is a mechanism through which electrons and holes of a semiconductor can be exchanged with an insulating interface due to the trap states located at the boundary between the semiconductor and the insulator. These trap states introduce energy levels within the energy gap of the semiconductor, which can be of donor or acceptor (or both) type. An example of energy band diagram which corresponds to the silicon-Si_{3N4} interface is schematically shown in Fig. 10(b). Here, the top electrode is grounded, while a voltage can be applied at the bottom electrode. Our silicon wafer is slightly p-doped (10^{16} cm^{-3}), so it has the Fermi level close to the top of the valence band. The energy levels within the bandgap are acceptors, i.e., they are empty and can be occupied by electrons from the valence band of silicon when a positive bias is applied. The number of traps in the energy interval between E and $E + dE$ is $D_t(E)dE$. When a positive voltage is applied, the Fermi level is pushed toward the lowest energy trap states (Fig. 10(c)), and electrons fill the trap states tunneling from the valence band of the semiconductor. As a result, holes will form in silicon. When the applied voltage is negative, the Fermi level is pulled away from the lowest energy trap states (Fig. 10(d)), so no holes are created. This could explain the asymmetric resonance shift observed in Fig. 7(a) between positive and negative values of V_{DC}. A fixed surface charge can be present at the Si_3N_4 interface, which induces band bending when no voltage is applied (10(e)). In this case the flat band condition is reached if a positive/negative (de-

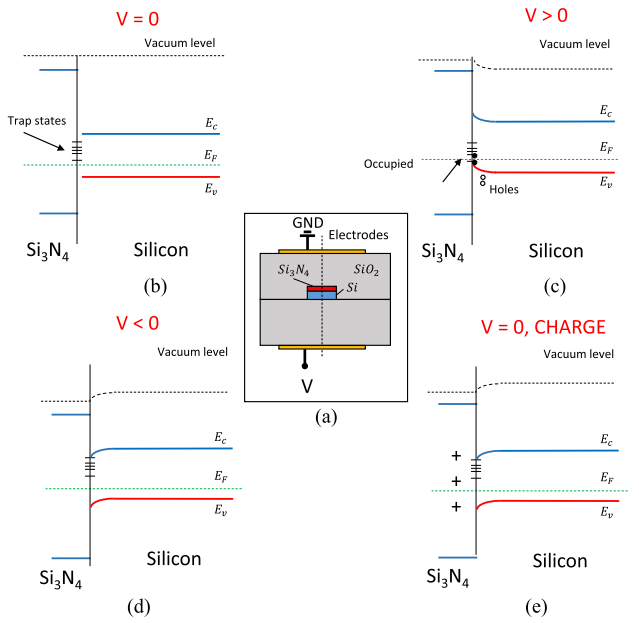

Fig. 10. (a) Cross section of the waveguide in the resonator, with the different layers and materials. (b) Energy band diagram of the $\mathrm{Si}-\mathrm{Si_3N_4}$ interface when no voltage is applied. This is the flat band condition. (c) Energy band diagram of the $\mathrm{Si}-\mathrm{Si_3N_4}$ interface when a positive voltage is applied, showing the release of holes from the trap states. (d) Energy band diagram of the $\mathrm{Si}-\mathrm{Si_3N_4}$ interface when a negative voltage is applied. (e) Energy band diagram of the $\mathrm{Si}-\mathrm{Si_3N_4}$ interface when no voltage is applied but a positive charge layer is present at the interface. Panels from (b) to (e) refer to the band diagrams along the vertical black dashed line of panel (a). E_c = conduction band, E_v = valence band, E_F = Fermi level.

pending on the surface charge sign) is applied. This is similar to what happens in a Metal Oxide Semiconductor capacitor in which trapped charges are present within the oxide layer [28]. The concentration of injected holes ΔP as a function of the applied voltage V_{DC} can be obtained by using the relation:

$$\Delta P(V_{DC}) = \int_{E_v}^{E_c} D_t(E) f_T(E, E_F(V_{DC}))\, dE \qquad (18)$$

where $f_T(E, E_F(V_{DC}))$ describes the occupancy of the energy level E. Depending on the trap density distribution, the hole contentration ΔP can be a nonlinear function of V_{DC}. The same discussion applies in case of donor traps, in which the occupancy f_T in (18) should be replaced with $(1 - f_T)$. Donor traps are probably the cause of the electro-optic behaviour shown in Fig. 5, since as shown in Fig. 9(a), the asymmetry can be accounted only by the injection of electrons. The fact that these are injected for both positive and negative voltages can be explained from the fact that we have two interfaces, one at the top of the waveguide between Silicon and $\mathrm{Si_{3N4}}$, and one at the bottom between Silicon and Silica. If both possess trap states of donor type, one interface releases electrons at positive voltages, while the other at negative ones. Depending on the trap type and distribution, the presence of two interfaces allows to inject electrons and/or holes with the same sign of the applied voltage, thus justifying the simulations in Fig. 9. The nonlinear injection of free carriers through STD can thus account for all the anomalies discussed in section IV. The trap density $D_t(E)$ is closely related to the type and quality of the interface. This is not easily controlled during fabrication. As a result, each device has its own trap density distribution, and this could explain the random trends observed in the electro-optic modulation shown in Fig. 4. The trap density associated to the silicon-silica interface is probably lower than the one of the silicon-$\mathrm{Si_{3N4}}$. This could explain why the samples without the stressing layer exhibited an electro-optic modulation which was an order of magnitude lower with respect to the ones covered with $\mathrm{Si_3N_4}$.

VIII. Conclusion

In this work, we probed the electro-optic response of strained silicon racetrack resonators, with the aim to determine the mechanism which is responsible of the modulation. To this purpose, a sinusoidal, low frequency (KHz) voltage applies an electric field across a portion of the resonator, and the amplitude of the first and second harmonic components of the transmitted optical signal is detected using a Lock In amplifier. Several devices exhibited an electro-optic response which is compatible with the linear Pockels effect, with $\chi^{(2)}$ values ranging from few pm/V up to 600 pm/V. However, the lack of a clear trend of these values with the waveguide width or with the crystallographic direction, suggested that the modulation mechanism is probably not related to strain induced second order nonlinearities. These doubts are supported by the observation of voltage induced absorption and of electro-optic responses which are strongly nonlinear with the applied voltage. We quantitatively proved that losses and refractive index shift are related, and that these can be attributed to the injection of free carriers in the waveguide in response to an applied electric field. The most plausible injection mechanism is p-type Surface Transfer Doping with the $\mathrm{Si_{3N4}}$ interface which covers the waveguide. Depending on the trap state distribution, the relation between the injected carriers and the applied voltage can be nonlinear, thus justifying the anomalous responses showed by some devices. Since STD is intrinsically related to the interface quality, which is not easily controllable during fabrication, the strength of the electro-optic response mediated by free carriers appears as randomly distributed across the wafer. In conclusion, this work constitutes a clear evidence that, at low frequency, the electro-optic modulation has to be attributed to free carrier effects, rather than $\chi^{(2)}$ nonlinearities. Despite this fact, the engineering of the interface quality could be instrumental for the realization of a low frequency (KHz–MHz) electro-optic modulator based on STD. Indeed, it is demonstrated that an equivalent $\chi^{(2)}$ at the order of 600 pm/V can be achieved, without the need of integration of pn-junctions on the chip.

Appendix A
Screening Effects Induced by Free Carrier Injection

In order to model the relation between the electric field inside the waveguide and the applied voltage in the presence of free carriers, we performed a FEM simulation in which the Poisson's equation for the field is coupled to the rate equations for free carriers [28]. The carrier injection is phe-

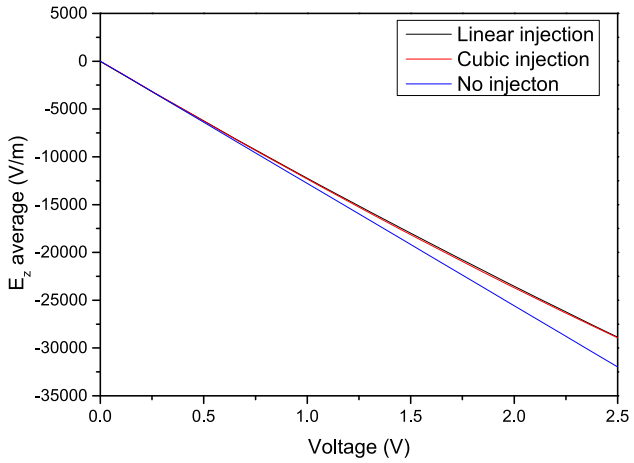

Fig. 11. Average of the $\hat{z}$ component of the electric field inside the waveguide as a function of the applied voltage. The black line comes from a linear injection model, the red line from a cubic model, while the blue line assumes no injection.

nomenologically introduced by letting the concentration of acceptor impurities N_A to be voltage dependent, in the form $N_D(V) = N_{D0} + d_1 V + d_2 \mathrm{V}^3$, with $N_{D0} = 10^{16}\,\mathrm{cm}^{-3}$. The coefficients d_1 and d_2 are found by considering the fact that, from Fig. 8(b), $N_D(V = 70\ \mathrm{V}) = 7.67 \cdot 10^{16}\ \mathrm{cm}^{-3}$, and that from Table I, $\frac{a1}{a3} \sim 25$. This gives $d_1 = 0.75 \cdot 10^{15}\ \mathrm{V}^{-1}\mathrm{cm}^{-3}$ and $d_2 = 0.03 \cdot 10^{15}\ \mathrm{V}^{-3}\mathrm{cm}^{-3}$. The modelled waveguide has a width of $w = 1.2\ \mu$m. The average of the $\hat{z}$ component of the electric field inside the waveguide, as a function of the voltage, is shown in Fig. 11. To show the screening effect, we reported also the curve when no carriers are injected. The data is then fitted by the second order polynomial $E(V) = c_1 V + c_2 \mathrm{V}^2$. The values of the two coefficients are $c_1 = (-12890 \pm 20)\ \mathrm{m}^{-1}$ and $c_2 = (520 \pm 6)\ \mathrm{m}^{-1}\mathrm{V}^{-1}$.

APPENDIX B
MODELING OF FREE CARRIER EFFECTS

A. Resonance Shift and Change in the Quality Factor

In order to monitor the resonance shift and the decrease of the quality factor induced by the injection of free carriers, the starting point are the Soref's equations [27]:

$$\begin{aligned} \Delta n &= -8.8 \cdot 10^{-22} \Delta N - 8.5 \cdot 10^{-18} \Delta P^{0.8} \\ \Delta \alpha &= 1.45 \cdot 10^{-17} (\Delta N + \Delta P) \end{aligned} \tag{19}$$

in which Δn and $\Delta \alpha$ are the changes in the refractive index and in the absorption coefficient of the material as a consequence of an electron(hole) concentration $\Delta N(\Delta P)$. These are translated into an effective index change Δn_{eff} and into an effective absorption $\Delta \alpha_{\mathrm{eff}}$ variation as [22]:

$$\begin{aligned} \Delta n_{\mathrm{eff}} &= \frac{\Gamma_c \Delta n}{n_0} n_g \\ \Delta \alpha_{\mathrm{eff}} &= \frac{\Gamma_c \Delta \alpha}{2 n_0} n_g \end{aligned} \tag{20}$$

in which Γ_c is the modal confinement factor. The resonance shift is obtained by plugging (20) into (8). The quality factor Q of an Add-Drop resonator has the analytical expression [21]:

$$Q = \frac{\pi n_g L \sqrt{1-\kappa^2}\sqrt{\tau}}{(1-(1-\kappa^2)\tau \lambda_m} \tag{21}$$

where L is the resonator perimeter and $\tau = \tau_0 e^{-\Delta \alpha_{\mathrm{eff}} L_h}$. The quantity τ_0 represent the roundtrip loss when no carriers are injected, while L_h is the length of the region in which the change in the absorption occurs (this is assumed to coincide with the electrode length). The parameters used to simulate the curves in Fig. 8 are listed in Table III.

TABLE III
LIST OF THE PARAMETERS USED TO SIMULATE THE CURVES IN FIG. 8

Parameter	Value	Source
κ^2	0.025	FEM simulation
n_g	4.24	FEM simulation
τ_0	0.9	Experiment
Γ_c	0.705	FEM simulation
$\lambda_{\mathrm{res},0}$	$1.5294\,\mu$m	Experiment
n_0	3.485	[24]

B. Modeling of the Electro-Optic Response

The curves shown in Fig. 9 are obtained by using (11). The wavelength dependence of $I_D(\omega)$ is implicit in the terms $\frac{\partial I_D}{\partial \lambda_m}$ and $\frac{\partial I_D}{\partial A}$, whose expression can be derived by differentiating (1) with respect to λ_m and A respectively. In order to compute the terms $\frac{\partial \lambda_m}{\partial V}$ and $\frac{\partial A}{\partial V}$, one needs an explicit expression which relates the applied voltage to the concentration of free carriers inside the waveguide. Once that this expression is known, it is possible to compute the amplitude and the resonance wavelength as a function of the applied voltage by using (19), (20) and the equations reported, e.g., in [29], for the maximum of the Drop signal. Some insights on the relation between the carrier concentration and the voltage can be extracted from Fig. 5(d). By integrating this curve with respect to V, it comes out that $A(V)$ can be well approximated by a quadratic relation (its derivative is almost a straight line), with a maximum at $V = 0$. This means that the dependence of the carrier concentration $\Delta N(\Delta P)$ with the applied voltage is also reasonably quadratic, in the form $\Delta N(\Delta P) = q\mathrm{V}^2$, where q is a constant that regulates the amount of injected carriers. At this point, this quantity does not significantly alter the relative magnitude between $\frac{\partial A}{\partial V}$ and $\frac{\partial \lambda_m}{\partial V}$. We choose a value of $\Delta N(\Delta P) = 10^{16}\ \mathrm{cm}^{-3}$ at $V = \pm 20$ V, which gives $q = 2.5 \cdot 10^{13}\ \mathrm{V}^{-2}\mathrm{cm}^{-3}$. The quadratic relation between $\Delta N(\Delta P)$ and V makes $\frac{\partial A}{\partial V}$ and $\frac{\partial \lambda_m}{\partial V}$ to decrease as V approaches zero. This is why in Fig. 9, the magnitude of the electro-optic response decreases as $V \to 0$.

REFERENCES

[1] C. L. Manganelli, P. Pintus, and C. Bonati, " Modeling of strain-induced Pockels effect in silicon," *Opt. Express*, vol. 23, pp. 28649–28666, 2015.
[2] P. Damas, D. Marris-Morini, E. Cassan, and L. Vivien, "Bond orbital description of the strain-induced second-order optical susceptibility in silicon," *Phys. Rev. B*, vol. 93, 2016, Art. no. 165208.

[3] M. Cazzanelli and J. Schilling, "Second order optical nonlinearity in silicon by symmetry breaking," *Appl. Phys. Rev.*, vol. 3, 2016, Art. no. 011104.
[4] E. L. Wooten *et al.*, "A review of lithium niobate modulators for fiber-optic communications systems," *IEEE J. Sel. Top. Quantum Electron.*, vol. 6, no. 1, pp. 69–82, Jan./Feb. 2000.
[5] B. E. Saleh, M. C. Teich, and B. E. Saleh, *Fundamentals of Photonics*. New York, NY, USA: Wiley, 1991.
[6] R. W. Boyd, *Nonlinear Optics*. New York, NY, USA: Academic, 2003.
[7] L. Pavesi and G. Guillot, "Optical interconnects," (Springer Series in Optical Sciences). New York, NY, USA: Springer, vol. 119, 2006.
[8] L. Pavesi, and D. J. Lockwood, *Silicon Photonics*. New York, NY, USA: Springer., vol. 1, 2004.
[9] R. S. Jacobsen *et al.*, "Strained silicon as a new electro-optic material," *Nature*, vol. 441, pp. 199–202, 2006.
[10] B. Chmielak *et al.*, "Investigation of local strain distribution and linear electro-optic effect in strained silicon waveguides," *Opt. Express*, vol. 21, pp. 25324–25332, 2013.
[11] B. Chmielak *et al.*, "Pockels effect based fully integrated, strained silicon electro-optic modulator," *Opt. Express*, vol. 19, pp. 17212–17219, 2011.
[12] M. W. Puckett, J. S. T. Smalley, M. Abashin, A. Grieco, and Y. Fainman, "Tensor of the second-order nonlinear susceptibility in asymmetrically strained silicon waveguides: analysis and experimental validation," *Opt. Lett.*, vol. 39, pp. 1693–1696, 2014.
[13] P. Damas *et al.*, "Wavelength dependence of pockels effect in strained silicon waveguides," *Opt. Express*, vol. 22, pp. 22095–22100, (2014).
[14] M. Cazzanell *et al.*, "Second-harmonic generation in silicon waveguides strained by silicon nitride," *Nat. Mater.*, vol. 11, pp. 148–154, 2012.
[15] S. Azadeh, F. Merget, M.P. Nezhad, and J.Witzens,"On the measurement of the Pockels effect in strained silicon," *Opt. Lett.*, vol. 40, pp. 1877–1880, 2015.
[16] R. Sharma, M. W. Puckett, H. H. Lin, A. Isichenko, F. Vallini, and Y. Fainman, "Effect of dielectric claddings on the electro-optic behavior of silicon waveguides," *Opt. Lett.*, vol. 41, pp. 1185–1188, 2016.
[17] M. Borghi *et al.*, "High-frequency electro-optic measurement of strained silicon racetrack resonators," *Opt. Letters*, vol. 40, pp. 5287–5290, 2015.
[18] P. Zhang *et al.*, "Electronic transport in nanometre-scale silicon-on-insulator membranes," *Nature*, vol. 439, pp. 703–706, 2006.
[19] L. Alloatti, C. Koos, and J. Leuthold, "Optical loss by surface transfer doping in silicon waveguides," *Appl. Phys. Lett.*, vol. 107, 2015, Art. no. 031107.
[20] J. Ristein, "Surface transfer doping of semiconductors," *Science*, vol. 313, pp. 1057–1058, 2006.
[21] W. Bogaerts *et al.*, "Silicon microring resonators," *Laser & Photon. Rev.*, vol. 6, pp. 47–73, 2012.
[22] R. Osgood *et al.*, "Engineering nonlinearities in nanoscale optical systems: Physics and applications in dispersion engineered silicon nanophotonic wires," *Adv. Opt. Photon.*, vol. 1, pp. 162–235, 2009.
[23] G. T. Reed, and A.P. Knights, *Silicon Photonics: An Introduction*. Hoboken, NJ, USA: Wiley, 2004.
[24] C. D. Salzberg and J. J. Villa, "Infrared refractive indexes of silicon germanium and modified selenium glass," *J. Opt. Soc. Amer.* A, vol. 47, pp. 244–246, 1957.
[25] C. Castellan, S. Tondini, M. Mancinelli, C. Kopp, and L. Pavesi, "Reflectance reduction in a whiskered SOI star coupler," *IEEE Photon. Technol. Lett.*, vol. 28, no. 17, pp. 1870–1873, Sep. 2016.
[26] C. Schriever *et al.*, "Second-order optical nonlinearity in silicon waveguides: Inhomogeneous stress and interfaces," *Adv. Opt. Mater.*, vol. 3, pp. 129–136, 2015.
[27] R. A. Soref, and B. R. Bennett, "Electrooptical effects in silicon," *IEEE J. Quantum Electron.*, vol. 23, no. 1, pp. 123–129, Jan. 1987.
[28] S. M. Sze, and K. K. Ng, *Physics of Semiconductor Devices*. Hoboken, NJ, USA: Wiley, 2006.
[29] W. Bogaerts *et al.*, "Silicon microring resonators," *Laser Photon. Rev.*, vol. 6, pp. 47–74, 2012.

Massimo Borghi received the B.S. degree in physics from the University of Modena and Reggio Emilia, Italy, in 2010, the M.S. degree in experimental physics in 2012 and the Ph.D degree in physics in 2016, both from the University of Trento, Italy. Since 2016, he has been a Post-Doc in physics in the Nanoscience Laboratory, University of Trento, Trento, Italy. His research interests include passive integrated networks involving single and coupled resonators, nonlinear Silicon photonic devices for frequency up/down conversion, electro-optic effects in strained silicon devices, and quantum optics in both free space and integrated silicon on insulator circuits.

Mattia Mancinelli received the B.S. degree in physics from the University of Perugia, Italy, in 2008, the M.S. degree in experimental physics in 2010, and the Ph.D. degree in physics in 2013, both from the University of Trento, Italy. Since 2013, he has been a Post-Doc in physics in the Nanoscience Laboratory, University of Trento. His research interests include coupled microresonators configurations to be used for signals processing in the linear and nonlinear regime and for on-chip generation of disordered bit, parametric conversion of the light and supecontinuum generation, and generation of correlated photon pairs exploiting a second order or third order parametric process in suitably designed silicon waveguides.

Martino Bernard received the B.S. degree in physics in 2011 and the M.S. degree in experimental physics in 2013 from the University of Trento, Italy. Since 2013, he has been working toward the Ph.D. degree at the University of Trento, working in the Centre of Materials and Microsystems, Bruno Kessler Foundation. His research interests include passive photonic integrated resonator circuits in silicon and glass-based materials with particular focus on Fano interference effects within these devices.

Mher Ghulinyan received the M.S. degree in 1995 and the Ph.D degree in 1999 from the Yerevan State University, Armenia. He is an R&D Researcher in the Centre of Materials and Microsystems, Bruno Kessler Foundation and a Contract Professor of physics at the University of Trento, Trento, Italy. In 2002, he moved to the University of Trento to join the Nanoscience Laboratory, working on silicon photonics research. His four years of research on 1-D optical superlattices (OSLs) paved the way for the first-time demonstrations of fundamental phenomena: photonic Bloch oscillations, resonant Zener tunneling, Anderson localization of light in random OSLs, the observation of optical necklace states, optical switching using capillary condensation, slow light propagation through OSLs, and the new concept of wavelength conversion in OSLs and light transport through Fibonacci quasi-crystals. In 2006, he moved to R&D research at the Bruno Kessler Foundation, joining the newely established Advanced Photonics & Photovoltaics group to work on integrated photonic systems. His main research interests include field of resonator optics, with a particular focus on monolithically integrated optically active and passive planar microresonators. He has authored one book and several book chapters, more than 60 papers, and one patent. He is member of OSA and is a frequently invited speaker at international conferences.

Georg Pucker received the Ph.D. degree in technical chemistry from Technical University in Graz, Austria, in 1996. He is a Senior Researcher in the Center of Materials and Microsystems, Bruno Kessler Foundation (FBK-CMM), Trento, Italy, and the Head of the research unit Advanced Functional Materials. From 1996 to 2001, he was in the Department of Physics, University of Trento, Italy, working on optical properties and structures of rare-earth-doped glasses and silicon nanostructures. Since 2001, he has been employed at FBK-CMM where he worked first on the development of radiation hard detectors for experiments in high-energy physics, then on silicon photonics with a focus on silicon nanostructures, nonlinear optical properties in silicon, and optical planar lightwave circuits for optical sensing. He coauthored more than 100 journal articles and conference proceedings and authored two patents and a book chapter.

Loren zo Pavesi (M'08–SM'11) was born in 1961. He received the Ph.D. degree in physics from the Ecole Polytechnique Federale of Lausanne, Switzerland, in 1990. He is a Full Professor of experimental physics, the Director of the Nanoscience Laboratory, and the Head of the Department of Physics, University of Trento, Trento, Italy. He is the author or coauthor of more than 300 papers, author of several reviews, editor of more than 10 books, author of 2 books, and holds 7 patents. His research interests include silicon-based photonics. He was the first President and Founder of the IEEE Italian chapter on Nanotechnology. During the last years, he is Chief Speciality Editor of the section Optics and Photonics of Frontiers in Materials, in the editorial board of Research Letters in Physics and he was in the editorial board of *Journal of Nanoscience and Nanotechnologies*, in the directive council of the LENS, Florence, italy, in the Board of Delegates of E-MRS. In 2001, he received the title of Cavaliere by the Italian President for scientific merit. In 2010 and 2011, he was elected Distinguished Speaker of the IEEE- Photonics society.